Visual Contrast Sensitivity Correlates to the Retinal Degeneration in Rhodopsin Knockout Mice

Jiaxin Xiao,[1,2] Muhammed Yasin Adil,[1,2] Karen Chang,[1,3] Zicheng Yu,[1] Lanbo Yang,[1] Tor P. Utheim,[4] Dong Feng Chen,[1] and Kin-Sang Cho[1,5]

[1]Schepens Eye Research Institute of Massachusetts Eye and Ear, Department of Ophthalmology, Harvard Medical School, Boston, Massachusetts, United States
[2]Faculty of Medicine, University of Oslo, Oslo, Norway
[3]National Taiwan University, Taiwan
[4]Department of Oral Biology, Faculty of Dentistry, University of Oslo, Norway
[5]Geriatric Research Education and Clinical Center, Office of Research and Development, Edith Nourse Rogers Memorial Veterans Hospital, Bedford, Massachusetts, United States

PURPOSE. Clinical manifestations of photoreceptor degeneration include gradual thinning of the outer nuclear layer (ONL) and progressive reduction of electroretinogram (ERG) amplitudes and vision loss. Although preclinical evaluations of treatment strategies greatly depend on rodent models, the courses of these changes in mice remain unclear. We thus sought to investigate the temporal correlations in changes of spatial vision, ERG response, and ONL thickness in mice with progressive photoreceptor degeneration.

METHODS. Adult wild-type (WT) mice and mice carrying rhodopsin deficiency ($Rho^{-/-}$), a frequently used mouse model of human retinitis pigmentosa, were selected for investigation. Mouse spatial vision, including visual acuity (VA) and contrast sensitivity (CS), was determined using optomotor response (OMR) assays; ONL thickness was quantified by spectral-domain optical coherence tomography (SD-OCT), and ERG was performed to evaluate retinal functions. The mice were killed when they were 14 weeks old, and the cone photoreceptors in retinal sections were counted.

RESULTS. Spatial vision, ONL thickness, and ERG amplitudes remained stable in WT mice at all examined time points. While 6-week-old $Rho^{-/-}$ mice had VA, CS, as well as ERG responses similar to those of WT mice, progressive reductions in the spatial vision and retinal functions were recorded thereafter. Most tested 12-week-old $Rho^{-/-}$ mice had no visual-evoked OMR and ERG responses. Moreover, CS, but not VA, displayed a linear decline that was closely associated with ONL thinning, reduction of ERG amplitudes, and loss of cones.

CONCLUSIONS. We presented a comprehensive study of the relation between the changes of spatial vision, retinal function, and ONL thickness in postnatal week (PW)6 to PW12 $Rho^{-/-}$ mice. CS is a more sensitive indicator of spatial vision compared to VA, although both are required as separate parameters for monitoring the visual changes in retina undergoing photoreceptor degeneration.

Keywords: rhodopsin deficiency mice, photoreceptor degeneration, visual performance

Photoreceptor degenerative diseases, including age-related macular degeneration, diabetic retinopathy, and retinitis pigmentosa (RP), represent the most common irreversible sight-threatening conditions. Among these diseases, RP includes a set of hereditary disorders that cause retinal degeneration, featured by progressive loss of rod and cone photoreceptors.[1,2] Therapeutics, such as stem cell and neuroprotective/regenerative strategies and gene targeting, bring hopes of slowing neurodegeneration or restoring vision. These technologies are under intensive investigation in animals, particularly mouse models, and their development demands clinically relevant morphologic and behavioral tests/assays for evaluating structural and visual function recovery or restoration. Currently, however, it remains unclear how the temporal changes in retinal function and spatial vision relate to photoreceptor loss in mice.

Animal models of RP are valuable tools for understanding the pathophysiology of degeneration, and yield important information on treatment development. Humphries et al.[3] introduced a mouse strain with rhodopsin deficiency ($Rho^{-/-}$) in 1997, which has since been frequently used in studying the pathogenesis of RP.[4–7] Partly, this is also because mutation of the Rho gene accounts for about 25% of dominant RP cases.[1] This mouse strain shows a complete absence of functional rhodopsin at birth and therefore establishes rod dysfunction. Rod photoreceptors in this mutant undergo degeneration around postnatal day 14,[4] and subsequently cone survival will be compromised.[3,4,6] The pattern of photoreceptor degeneration in $Rho^{-/-}$ mice is similar to that in patients with RP, which makes this mouse strain a convenient model for investigating RP pathogenesis and designing treatment for RP.

In the clinic, retinal degeneration is evaluated by electro-retinogram (ERG), spectral-domain optical coherence tomography (SD-OCT), and optomotor response (OMR).[8] The morphological changes and ERG responses in patients are often diminished long before visual symptoms, including decreased visual acuity (VA) or contrast sensitivity (CS), arise.[1] For evaluating treatment responses, it is therefore important to fully explore both functional and structural changes in animal models of RP, such as $Rho^{-/-}$ mice. Although the retinal function and morphologic changes in the $Rho^{-/-}$ mouse model have been reported in other studies,[3–7,9–16] assessments of these parameters are usually carried out separately; the relations between spatial vision of CS, VA, and retinal function and photoreceptor loss remain unclear. To our knowledge, this is the first study to comprehensively examine and correlate the changes of spatial vision, retinal function, and photoreceptor loss in the $Rho^{-/-}$ mouse model of RP.

In animal models, the spatial vision is normally assessed by reflex that serves to stabilize the visual image on the retina during locomotion.[9,16–20] These reflexes are mediated through accessory optic system,[21] without visual cortex processing, and elicit compensatory head movements (OMR) in unrestrained animals[9,16,20] or eye movements (optokinetic response, OKR) in head-fixed animals[17,18] exposed to globally rotating striped patterns. The setup of OMR is easy to build and it is a simple approach to evaluate the visual function of mice without prior training.

The aim of the present study was to investigate the spatial vision in $Rho^{-/-}$ mice by assessing VA and CS, the gold standard for clinical assessment of vision, using a visual behavioral test based on OMR. More specifically, we evaluated the relationship between the changes in spatial vision, survival of photoreceptors, and ERG responses. This comprehensive study will expand insights into the progressive retinal degeneration in the $Rho^{-/-}$ mouse model.

METHODS

Animals

$Rho^{-/-}$ mice carrying C57BL/6 background (a gift from M. Young's lab at Schepens that was originally developed by Humphries and his team in Trinity College, Dublin) aged 6 to 12 weeks were used in this study. Adult C57BL/6 wild-type (WT) mice (Jackson Laboratory, Bar Harbor, ME, USA) aged 6 to 14 weeks were used as the control. The mice were monitored longitudinally with live retinal imaging using SD-OCT, ERG, and OMR. At the end point, mice were killed, and eyeball sections were processed for immunolabeling of cone opsin. All animal experiments were performed in accordance with the protocols approved by the Institutional Animal Care and Use Committee of the Schepens Eye Research Institute and adhered to the ARVO Statement for the Use of Animals in Ophthalmologic and Vision Research. The mice were kept in a 12-hour light/dark cycle with free access to food and water.

OMR-Based Visual Assessment

A setup of an OMR prototype was built as previously described.[16] Briefly, it consisted of a custom-built box with a pedestal located in the center of an enclosure formed by four identical, connected 17-inch liquid crystal display monitors that displayed moving black and white gratings (Fig. 1A). Whisper fans were placed behind the monitors for ventilation. The test procedure was started by placing a mouse on the pedestal; it was allowed to move freely while exposed to visual stimuli displayed on the monitors (Fig. 1A). The optomotor stimulus consisted of vertical sine-wave gratings that rotated at a constant speed (12°/s).[9,22–25] The direction of rotation was randomly selected and alternated between clockwise and counterclockwise. When a detectable stimulus was displayed, the mouse normally stopped moving and initiated head tracking, defined as a smooth reflexive head movement with a velocity and direction in concert with the rotation.[23,25] Two experienced observers recorded and verified the OMR of the mouse in a masked fashion, and a minimum three instances of head tracking observed by both observers was required to conclude that the animal could detect the stimulus. If an animal slipped or jumped off the platform during testing, it was returned to the pedestal and testing was resumed.

Spatial frequency thresholds were measured using the staircase paradigm.[26] While the sinusoidal gratings were at 100% contrast (black stripe, 0.3 cd/m²; white stripe, 205 cd/m²), their spatial frequency was systematically increased in successive trials until the animals ceased to track the moving stimulus. The highest response eliciting spatial frequency was defined as the animal's VA.[9,27] The CS threshold was determined by presenting sinusoidal gratings at a fixed spatial frequency, whereas the contrast was systematically reduced until the threshold was identified. The threshold was presented as Michelson contrast based on the screen's luminance (maximum − minimum)/(maximum + minimum), and CS was calculated from the reciprocal value of the threshold. To generate a CS function, the threshold was identified at five spatial frequencies (0.067, 0.133, 0.209, 0.266, 0.4 cycle per degree [cyc/deg]).

Electroretinogram

Mice were dark-adapted for at least 6 hours before ERG recording. All procedures were performed in a dark room with a red safety light. The mice were anesthetized by intraperitoneal injection of a mixed solution of ketamine (120 mg/kg) and xylazine (20 mg/kg), and the pupils were dilated using 1% tropicamide (Alcon, Lake Forest, IL, USA) eye drops. The anesthetized mice were placed on a 37°C warm pad in a Ganzfeld bowl (Diagnosys LLC, Lowell, MA, USA) while recording. Gold wire ring electrodes were placed on each cornea; silver needle electrodes served as reference and were inserted subcutaneously in the forehead and the back area near the tail. GenTeal lubricating gel (Alcon, Fort Worth, TX, USA) was applied on both corneas to keep the cornea moist. ERGs were recorded from both eyes simultaneously. Both single-flash and flicker recordings were obtained under photopic condition. Single-flash stimuli were presented with a light intensity of 3.0 cd·s/m², while flicker stimuli had an intensity of 10.0 cd·s/m² with frequencies of 3, 10, and 15 Hz. The a-wave amplitude was measured from the baseline to the cornea-negative peak, and b-wave amplitude was measured from the cornea-negative peak to the first major cornea-positive peak after oscillatory potentials.

SD-OCT Live Imaging of Retinal Lamination

SD-OCT was performed using a Bioptigen Spectral Domain Ophthalmic Imaging System (Bioptigen, Inc., Durham, NC, USA) as previously described.[28] The system has a platform designed for easy orientation and aligning of mice for retinal imaging, and provides a high resolution of 2 μm. The mice were anesthetized by intraperitoneal injection with a mixed solution of ketamine and xylazine. The pupils were dilated with 1% tropicamide eye drops prior to imaging. Radial volume scan (centered on the optic disc, consisting of 100 B-scans) was acquired using image analysis software (InVivoVue Clinic; Bioptigen, Durham, NC, USA). Outer nuclear layer (ONL)
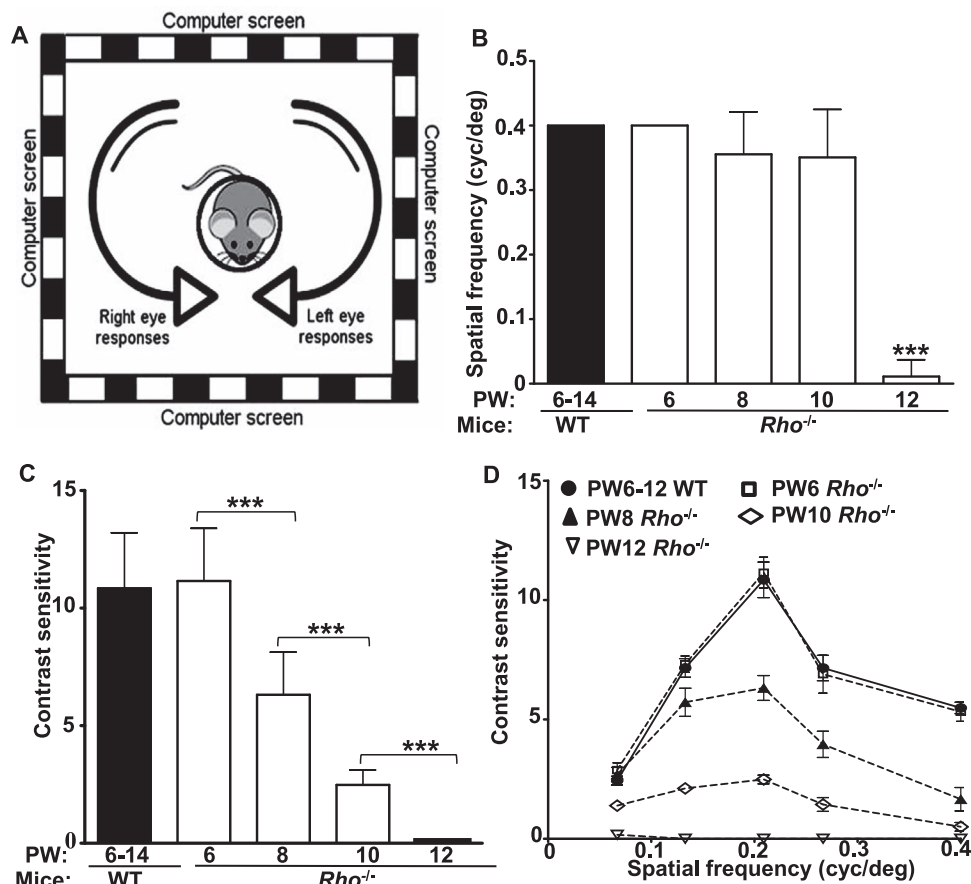
FIGURE 1. OMR-based VA and CS evaluation in $Rho^{-/-}$ mice. (**A**) Schematic representation of the OMR setup. A mouse is placed on the platform in the middle of an enclosed area surrounded by four identical computer screens. Vertical sine-wave gratings are projected on the screens and rotated at a constant speed of 12°/s. The spatial frequency and contrast of the grating are adjustable for measuring visual performance. The direction of rotation is alternated between clockwise and counterclockwise to test responses of the left and right eye, respectively. (**B**) Tracking of spatial frequency or VA in WT (*black bar*; $n = 10$) and $Rho^{-/-}$ (*white bars*; $n = 8$) mice. Note the drastic decrease of VA in PW12 $Rho^{-/-}$ mice. (**C**) Tracking of contrast sensitivity in WT (*black bar*; $n = 10$) and $Rho^{-/-}$ (*white bars*; $n = 8$) mice. Note the CS was evaluated at 0.209 cyc/deg. (**D**) Assessments of CS under various spatial frequencies in WT (*solid line*; $n = 10$) and $Rho^{-/-}$ mice (*dotted lines*; $n = 8$). Note the age-related decline of CS at all spatial frequencies. Peak CS assessed at the spatial frequency of 0.209 cyc/deg. ***$P < 0.001$.

thickness is an indicator of photoreceptor survival, and measurements were assessed using ImageJ (National Institutes of Health) software[29] on four selected scans (scan numbers 1, 26, 51, 76 represent 0°, 45°, 90°, and 135°, respectively, in en face images).[30] The lines defining ONL (between the outer plexiform layer to the outer limiting membrane) were drawn in ImageJ (2 μm/pixel), one on each side of the optic disc, 300 μm from the optic disc. The measurements of ONL thickness were performed by experienced investigators in a masked fashion.

Immunohistochemistry

As previously described,[31] mice were killed via CO_2 inhalation, followed by cervical dislocation. The eyes were enucleated and fixed in 4% paraformaldehyde overnight at 4°C. The fixed eyeballs were transferred into 20% sucrose in phosphate-buffered saline (PBS) at room temperature, followed by embedding in optimal cutting temperature compound (Tissue-Tek; Sakura, Torrance, CA, USA) and sectioned. Frozen 8-μm-thick sections containing the optic nerve were collected for immunolabeling. The retinal sections were blocked with PBS containing 0.3% Triton X-100 and 1% bovine serum albumin for 1 hour at room temperature, and then incubated with 1:200 rabbit anti-blue opsin (B-opsin) or rabbit anti-red/green opsin (R/G-opsin) overnight at 4°C. Both antibodies were purchased from EMD Millipore (Burlington, MA, USA). The sections were washed with PBS and then incubated with 1:200 Cy2-conjugated anti-rabbit IgG (Jackson ImmunoResearch, West Grove, PA, USA) for 2 hours at room temperature. Following washing in PBS, the sections were mounted using mounting medium with 4′,6-diamidino-2-phenylindole (DAPI; Abcam, Cambridge, MA, USA). Images were acquired on a fluorescence microscope (Leica, Bannockburn, IL, USA). The opsin-positive cells on each retinal section were counted, and at least three sections containing optic nerve from each mouse were selected for quantification. Three mice were included for each time point. The numbers of cones positive for B-opsin and/or R/G-opsin per retinal section were averaged per time point.

Statistical Analysis

Statistical analyses were performed using SPSS (v25.0; SPSS Inc., Chicago, IL, USA). Differences among multiple groups were compared using 1-way analysis of variance (ANOVA) and the Games-Howell post hoc test, and the difference between two groups was compared using the Mann-Whitney U test. $P < 0.05$ was considered statistically significant. Data are reported as the mean ± standard deviation unless otherwise specified.

RESULTS

Reduction of VA and CS in *Rho*$^{-/-}$ Mice

To determine how VA and CS change in *Rho*$^{-/-}$ and age-matched mice, we performed OMR assays to noninvasively assess mouse spatial vision. WT mice develop mature and stabilized vision around postnatal week (PW)6. The average VA of PW6 *Rho*$^{-/-}$ mice was ~0.4 cyc/deg, similar to that in the PW6 to 14 WT mice (Fig. 1B). The VA remained stable in WT mice throughout the study period, whereas that of *Rho*$^{-/-}$ mice remained constant up to PW10, but exhibited a drastic decline at PW12 (Fig. 1B), suggesting radical loss of visual function in these mice. In the same groups of WT and *Rho*$^{-/-}$ mice, we also tracked CS between PW6 and PW12. As spatial frequencies influence OMR-based CS assessment, we measured CS at five different spatial frequencies. In all mice, CS peaked at 0.209 cyc/deg at all time points examined (Fig. 1C). In agreement with the VA testing results, no significant differences in CS were noted between the PW6 WT (10.8 ± 2.4) and *Rho*$^{-/-}$ mice (11.1 ± 2.2). Thereafter, however, *Rho*$^{-/-}$ mice exhibited a gradual decline in CS at all spatial frequencies examined until it became flattened by PW12, when OMR-evoked head-tracking movements were no longer detectable in *Rho*$^{-/-}$ mice (Fig. 1C). A similar gradual decline of peak CS was noted in *Rho*$^{-/-}$ mice from PW6 to PW12 (Fig. 1D). These data indicate that *Rho*$^{-/-}$ mice had nearly normal vision at PW6 or VA and CS similar to values in WT mice, but became blind at about PW12. In *Rho*$^{-/-}$ mice, CS, especially peak CS change, was a more sensitive measure for the gradual visual decline than VA.

ERG Amplitude Declines in *Rho*$^{-/-}$ Mice

As retinal functions assessed by ERG declined in *Rho*$^{-/-}$ mice, deterioration of spatial vision of VA and CS also occurred along with photoreceptor degeneration; however, the exact relations between the amplitude of ERG response and VA or CS threshold changes remain unclear. Because all rod photoreceptors are dysfunctional in *Rho*$^{-/-}$ mice, absent of scotopic ERG response is expected.[4–7] Thus, we only recorded photopic responses of ERG, which measure the cone functions, in the above group of WT and *Rho*$^{-/-}$ mice from PW6 to PW12. As expected, PW6 *Rho*$^{-/-}$ mice displayed largely diminished a-wave due to rod dysfunction, but normal b-wave amplitude as compared to the WT mice (Figs. 2A, 2B). In light-adapted conditions, photopic 600 ERG showed similar responses in PW6 *Rho*$^{-/-}$ and WT mice (average, ~144 ± 9 and ~136 ± 6 μV, respectively), but the responses decreased in *Rho*$^{-/-}$ mice at later time points. Interestingly, *Rho*$^{-/-}$ mice first showed increased b-wave amplitudes at PW6 in 3-Hz flicker ERG recordings, which were averaged to ~140 ± 7 μV when it was ~120 ± 5 μV in PW6 WT mice ($P < 0.05$), likely indicative of a compensatory response in *Rho*$^{-/-}$ mice. Thereafter, b-wave amplitude in photopic 3-Hz flicker ERG recordings declined gradually until it became barely detectable at PW12. A similar response trend was seen in both 10- and 15-Hz flicker ERG recordings of the *Rho*$^{-/-}$ mice. These results suggest that the ERG signal is a sensitive measure for the progression of photoreceptor degeneration.

ONL Thinning and Cone Degeneration

Next, we studied how photoreceptor functional changes measured by ERG or VA and CS declines as determined by OMR relate to the loss of photoreceptors. Although most gene mutations that cause RP are rod photoreceptor–specific
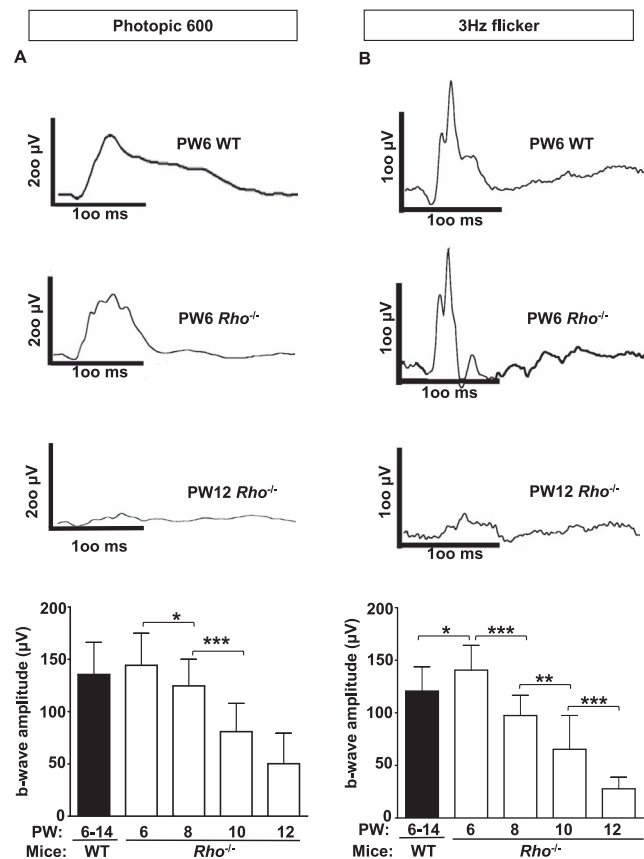

FIGURE 2. ERG recordings from C57BL/6 and *Rho*$^{-/-}$ mice in light-adapted conditions. **(A)** The waveform patterns and amplitudes of ERG recording in C57BL/6 (WT) mice were stable in photopic ERG (600 cd.s/m^2). In the *Rho*$^{-/-}$ mice, no obvious a-wave was observed **(B)** The waveform and amplitude of 3-Hz flicker ERG. The b-wave amplitude showed a supernormal function in the 3-Hz flicker recordings in 6-week-old *Rho*$^{-/-}$ mice (~140 ± 7 μV, $P < 0.05$ by ANOVA), but the signals were further progressively diminished up to week 12. *$P < 0.05$; **$P < 0.01$; and ***$P < 0.001$.

genes, cone photoreceptors die as a result of the loss of rods; nevertheless, whether the loss of cones correlates with the loss of rods, which is usually measured by reduction of ONL thickness in OCT, remains largely unknown. To address this question, we tracked ONL thickness in live *Rho*$^{-/-}$ and WT mice in the same group of mice described above. Moreover, at each time point examined, another group of mice were killed to examine for retinal histology and cone immunolabeling/quantification. At PW6, there was already >40% ONL thinning in the *Rho*$^{-/-}$ mice compared to the age-matched WT mice (Figs. 3A, 3B). As mouse retina contains two types of cones, that is, B-opsin and R/G-opsin, we counted both of them, respectively, in retinal sections. Accordingly, we observed >40% reduction of both B-opsin+ and R/G-opsin+ cones in PW6 *Rho*$^{-/-}$ mice compared to WT mice (Figs. 4A–D). As ERG and OMR assessments did not detect functional loss at this early time point, the data suggest that morphologic loss of photoreceptors occurs earlier than functional deterioration. Moreover, we showed that both ONL thickness and cone density decreased gradually in parallel from PW6 to PW12, indicating a close correlation between the reduction of cone density and ONL thickness (Fig. 4E) in *Rho*$^{-/-}$ mice.
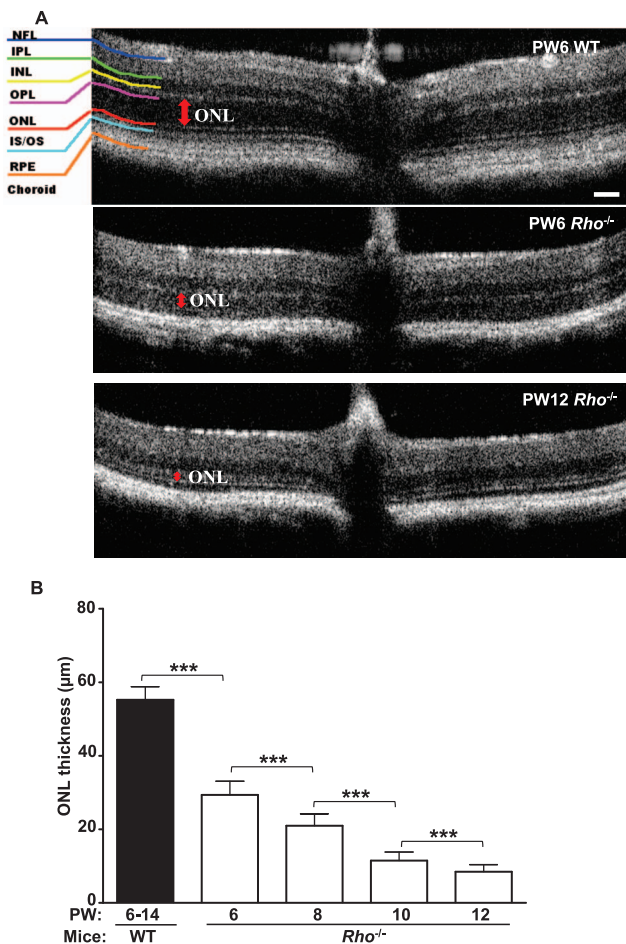
Figure 3. Cross-sectional OCT images. **(A)** Representative retinal B-scan images showing segmentation of SD-OCT images from WT and $Rho^{-/-}$ mice. *Red arrow* marks the thickness of outer nuclear layer. **(B)** Quantification the thickness of ONL. ***$P < 0.001$.

Relationships Among Visual Function, ERG, and Cone Photoreceptor Survival

To relate visual performance with ERG and histologic changes, we calculated the Pearson correlation coefficient (r) and linear regression slope for VA and CS versus ERG b-wave amplitude, and cone densities. A linear correlation was established between visual performance (CS and VA), retinal function, and morphology (Fig. 5). The gradual decline in CS in the $Rho^{-/-}$ mice was more strongly associated with other tested parameters (photopic 3-Hz flicker ERG, $r = 0.86$; cone cell survival, $r = 0.70$; both, $P < 0.001$). On the other hand, VA demonstrated weaker, but still significant, correlation to morphology and ERG recording (photopic 3-Hz flicker ERG, $r = 0.65$, $P < 0.01$; cone cell survival, $r = 0.52$, $P < 0.05$). Together these data suggest that CS may serve as a more sensitive functional measure for early loss of photoreceptor and retinal function than VA.

DISCUSSION

In the present study, the VA and CS thresholds were determined for a cohort of 6- to 12-week-old $Rho^{-/-}$ mice and were compared to those of WT adult C57BL/6 mice. The $Rho^{-/-}$ mice exhibited progressive loss of CS in 6 to 12 weeks; their VA was relatively stable until they were 12 weeks old.

Contrast sensitivity is a more sensitive indicator than VA in showing the functional decline of $Rho^{-/-}$ mice, while also showing a mild correlation to the changes of ERG and ONL thickness.

The OMR assay used in the present study is an established method that provides rapid assessment of spatial vision.[20,22–24,32,33] Due to its convenience and reproducibility, this method has been increasingly used to evaluate mouse vision. The assay is based on the principle of involuntary compensatory mechanisms for image stabilization during motion.[9,16,20] The vestibulo–ocular reflex integrates information to evoke eye movement, namely, OKR, or head movements/OMR, to serve the functional purpose of stabilizing images on the retina. Both OKR and OMR are mediated by retinal ganglion cells[34,35] sending information to the accessory optic system,[21] without an essential involvement of the visual cortex. Thus, the OMR assay in this study does not measure the visual perception processed through visual cortex.

Using the setup of OMR tests, we observed maximum VA at 0.4 cyc/deg in WT mice, which is consistent with the earlier studies.[9,27] Consistent with our recent report, the same VA threshold of 0.4 cyc/deg was found in 6-week-old $Rho^{-/-}$ mice. This finding contradicts the VA measured using optomotor drums by Schmucker et al.[36] The authors reported that the VA threshold of $Rho^{-/-}$ mice at a similar age (between 30 and 40 days) was only 0.1 cyc/deg. The experiments were, however, conducted under completely different light intensity, which most likely led to the variation in the VA. In the present study, $Rho^{-/-}$ mice showed stable VA under the photopic condition until they were 12 weeks old, when all animals lost the ability to detect the moving gratings, indicating a complete loss of spatial vision.

This observation differed from that of a previous report stating that less than 40% of tested PW13 $Rho^{-/-}$ mice still detected the visual stimuli using an automated algorithm for OMR detection.[9] Despite similar experimental setup and protocol, the visual stimuli in the present study had lower light intensity and could consequently be unable to activate the slightest residual cone function in this particular mouse model. The OMR is reduced with decreasing luminance, even in WT mice, and it is reasonable to speculate that the visual performance in $Rho^{-/-}$ mice would be even more sensitive to bright light intensity. A higher light intensity may be required to activate all residual cone function in this animal model. Moreover, the mouse's OMR responses will become less obvious as the visual performance weakens, and the weak OMR may be mixed with voluntary head movements and consequently lead to the conclusion of a visual threshold due to the sensitivity of an automated algorithm.

The CS in $Rho^{-/-}$ mice appeared to decrease gradually until week 12, when the visual performance was completely compromised. The finding in this animal model shares similar features to patients with RP, where CS measurements were reduced even when their VA losses were mild.[37–42] RP is a complex disease with a unique set of clinical characteristics that includes nyctalopia as the earliest symptom, diminution in wave amplitudes in ERG, and loss of VA in the late stage.[1] In patients, the measures of retinal function are diminished long before the visual symptoms arise.[1] The CS in the 6- to 14-week-old WT mice, on the other hand, did not demonstrate any age-related changes, although the results showed some discrepancy with the findings of Prusky et al.[9] This could be explained either by the different experimental protocol, or the fact that we assessed CS at different spatial frequencies. Nevertheless, both the CS and VA displayed great consistency within the same mouse strain. Taken together, our results suggest that CS is a more sensitive measurement of visual performance compared to VA.
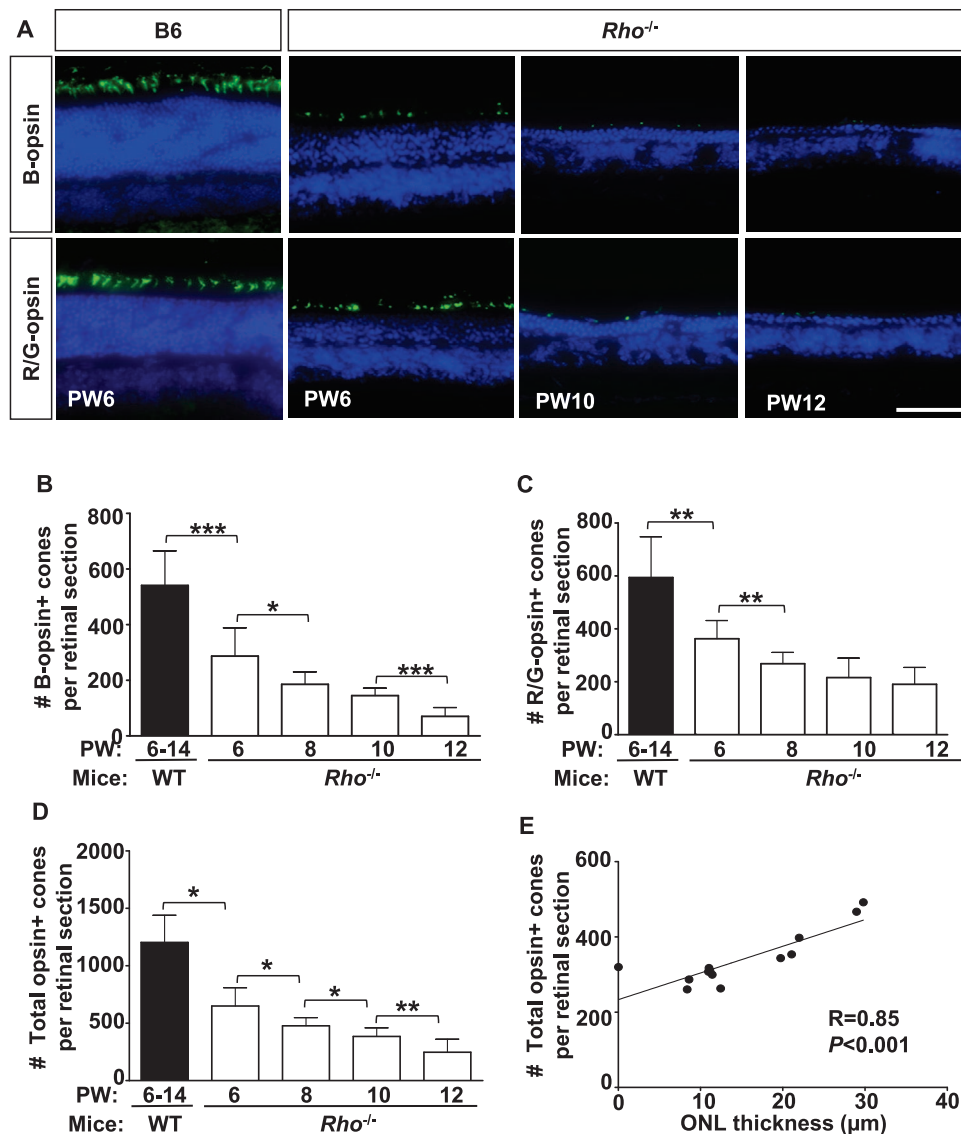
FIGURE 4. Quantification of opsin-positive cones and correlation to ONL thickness. (**A**) Immunolabeling of B-opsin and R/G-opsin on retinal sections of WT and $Rho^{-/-}$ mice. (**B–D**) Quantification of (**B**) B-opsin-, (**C**) R/G opsin-, and (**D**) total opsin-positive cells on retinal sections. (**E**) Scatter plot showing correlation between total number of opsin+ cones and ONL thickness. Note a significant positive association between ONL thickness by OCT imaging and the number of cones on retinal section. *Scale bar*: 50 μm.

In the $Rho^{-/-}$ mouse in which rod visual pigments are mutated, the rod-driven signals are completely abolished. The electrophysiological changes in this model have been characterized previously,[4-7] and no ERG response could be elicited in scotopic conditions (luminance lower than −2.0 log cd s/m²),[7,15] indicating that only the cone pathways contribute to ERGs. Thus, we mainly focused on the photopic ERG recordings, which measure the cone response. In the present study, the ERG signal was normal at PW6 $Rho^{-/-}$ mice compared to that in WT mice and gradually decreased until PW13, where no perceivable ERG response was detectable.[4] Interestingly, 6-week-old $Rho^{-/-}$ mice appeared to have significantly higher flicker ERG response under light-adapted conditions compared to the WT mice. This finding is in line with earlier reports[4,43] and suggests supernormal cone function in $Rho^{-/-}$ mice at 6 weeks. However, the ERG signals were significantly weaker at the later time points, indicating progressive loss of cone photoreceptor function.

Synaptic remodeling was reported in retina undergoing photoreceptor degeneration,[44] although the underlying mechanism remains unclear. In normal retina, rod bipolar cells solely form synapse with rod photoreceptor but not cones. The rod bipolar cells have plasticity remodeling by forming the synaptic connection to cones when the preferred cell type rod becomes unavailable in rd1 and $Rho^{-/-}$ mice.[45,46] Interestingly, no ectopic synapse was detected when both rod and cone photoreceptors became dysfunctional.[47] Thus, synaptic remodeling could change the structural basis for ERG and ONL measures. Although the underlying mechanism of synaptic remodeling remains unclear, the physiological activity of surviving photoreceptor may contribute to it. The transient increased cone function in Figure 3 could be a result of remodeling of cones and synaptic changes that start shortly after nonfunctional rods begin to degenerate. Degeneration and loss of photoreceptors lead to synaptic changes and remodeling of the second-order neurons, including axonal sprouting, progressive dendritic retraction, and ectopic synap-
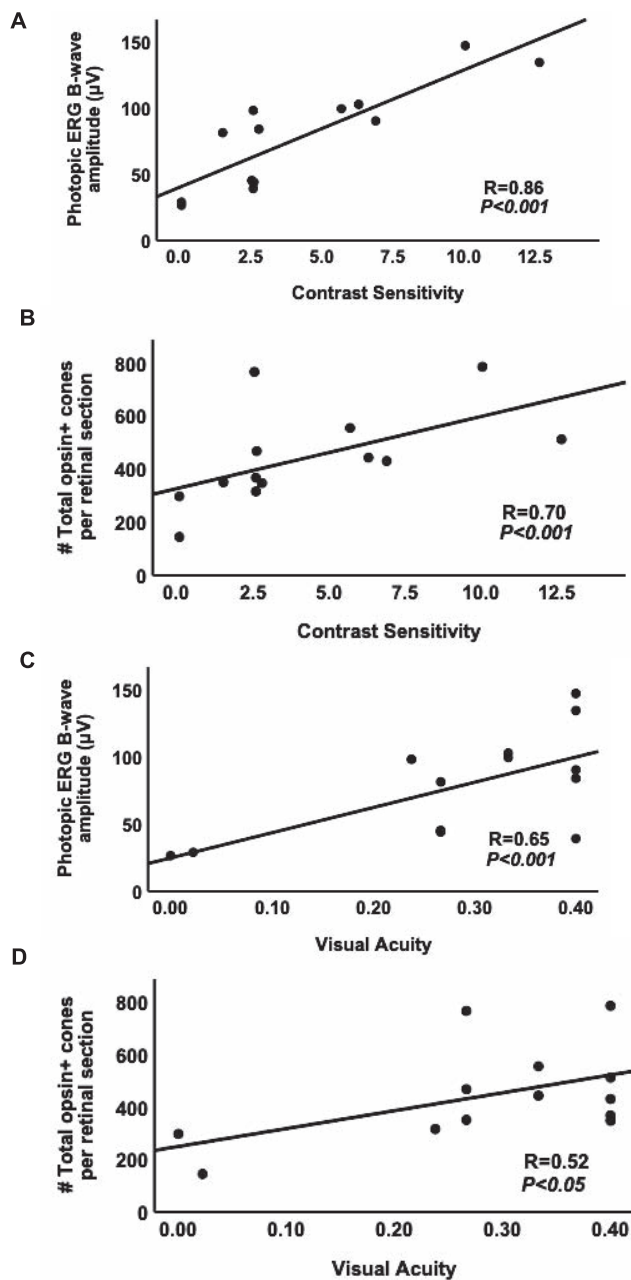
FIGURE 5. The relationship between visual performance, retinal morphology, and function. **(A–D)** Scatter plots showing correlation of CS and **(A)** photopic ERG and **(B)** total opsin+ cones, and correlation of VA and **(C)** photopic ERG and **(D)** total opsin+ cones. The correlation was performed on animals of same age. Note that the gradual decline in CS, rather than VA, showed a stronger linear association with b-wave amplitudes in photopic ERG and cone survival in $Rho^{-/-}$ mice. Note that the CS was evaluated at 0.209 cyc/deg.

togenesis.[44,48–52] In the process of remodeling, cone photoreceptors are able to substantially outgrow new processes after loss of outer segments.[52] Furthermore, rod bipolar cell dendrites that avoid cone photoreceptors in normal retinae are reported to form synapses with cones in $Rho^{-/-}$ mice retinae.[45,46]

The death of photoreceptors is a fundamental characteristic of RP. In the present study, we evaluated the retinal morphology by OCT imaging and histology. OCT is a noninvasive imaging approach that is commonly used to monitor the progress of retinal degeneration, and it has been proven to provide accurate and reliable measurements of retinal layers.[4] Our results revealed a significantly reduced ONL at PW6, consistent with a recent study.[6] The ONL thickness further shrank at each time point examined up to PW12. Although the ONL thickness is biased toward the surviving rod photoreceptors, our data suggest that it has a strong correlation to cone survival (Fig. 4E). There is a report showing a correlation of ONL thickness and cone density in normal eyes and eyes with RP.[53] In the normal human eye, this is in line with the idea that cone survival requires the support of trophic factors produced by rods[54]; thus, the degeneration of rods compromised the survival of cone photoreceptors in *Rho* knockout mice. Our data suggest the potential of utilizing OCT images in the clinic as indirect measurements/estimations for cone survival. Conversely, the ONL thickness in the WT mice was unchanged throughout the period examined from PW6 to 14. In $Rho^{-/-}$ mice, cone photoreceptor degeneration is known to follow the loss of dysfunctional rods. Therefore, the gradual drop in quantification of ONL thickness illustrates the loss of both nonfunctional rods and fully functional cone photoreceptors. Thus, to evaluate cone degeneration specifically, we also quantified the number of opsin-expressing cone photoreceptors. Our results on the WT mice are comparable to those of others.[55] In contrast, the opsin+ cone photoreceptors in the $Rho^{-/-}$ mice were significantly reduced at each time point and indicated a developmental degeneration of cones from 6 to 12 weeks. The data in Figure 4E represent the number of opsin+ cones per retinal section while we could not detect the thickness of ONL on the same retina by OCT. One possibility is that opsin signal is still present in the inner/outer segment but the cone nuclei were degenerated. Measuring the thickness of inner segment/outer segment (IS/OS) may reflect the thickness of a surviving cone but still not be necessary for the surviving cone. Technically, the OCT images of IS/OS and retinal pigment epithelium could sometimes fuse together, making it difficult to measure the thickness of IS/OS. Our data in Figure 4E suggest that the detection limit of ONL thickness of *Rho* knockout mice by OCT in our protocol is approximately 8 μm.

Although the ERG and morphologic changes in this mutant mouse model have been previously described,[4–7,10–15] the exact relation among the changes of spatial vision, ERG, and morphologic degeneration in $Rho^{-/-}$ mice remains unclear. In this study, we systematically characterized these changes in the same mice. We kept the spatial vision as an independent variable (x-axis) and asked if it could predict the changes of ERG or ONL thickness. We noticed that the correlation was significant but rather low; the changes of spatial vision could not quite predict retinal function (ERG) deterioration and the reduction of ONL thickness in $Rho^{-/-}$ mice or vice versa. This may be because the spatial vision is not only influenced by local retinal circuitry but also regulated by subcortical visual pathways.[56] Overall, our results suggest that CS and VA could not replace the ONL thickness quantification and ERG measurement, or vice versa. Compared to VA, CS is a more sensitive measure for detection of early vision deterioration, showing better correlation to the changes of ERG and ONL thickness. Assessment of spatial vision is important for drug development/evaluation of the effect of a potential drug to rescue vision in a mouse model of RP.

Figures 5C and 5D show that there are two subgroups. Unlike the gradual decline of CS in *Rho* knockout mice (Fig. 1C), the VA is rather similar to that in WT mice up to PW10 (Fig. 1D), and a significant decline was detected at PW12. In fact, this is in line with observations in RP patients.[57,58] The decline of CS is first detected in RP patents while the VA shows no significant changes. Our data suggest that there is a

threshold of the number of cones to maintain normal VA in $Rho^{-/-}$ mice that was reported in RP patients[59] or that our OMR setup is not sensitive enough to detect small changes of VA.

In summary, our study reveals that the time window of changes in visual performance in $Rho^{-/-}$ mice is between PW6 and PW12. In $Rho^{-/-}$ mice, CS is a more sensitive indicator of visual performance compared to VA. Moreover, the deterioration of the CS and VA threshold is not quite predictable by progressively diminished ERG signals and cone photoreceptor degeneration. Testing CS and VA is, therefore, required as a separate parameter for monitoring the visual changes in retinal degeneration and to serve as a sensitive readout for high-throughput drug screening for treating RP.

References

1. Hartong DT, Berson EL, Dryja TP. Retinitis pigmentosa. *Lancet*. 2006;368:1795–1809.

2. Fahim AT, Daiger SP, Weleber RG. Retinitis pigmentosa overview. In: Adam MP, Ardinger HH, Pagon RA, et al., eds. *GeneReviews*. Seattle, WA: University of Washington; 1993.

3. Humphries MM, Rancourt D, Farrar GJ, et al. Retinopathy induced in mice by targeted disruption of the rhodopsin gene. *Nat Genet*. 1997;15:216–219.

4. Jaissle GB, May CA, Reinhard J, et al. Evaluation of the rhodopsin knockout mouse as a model of pure cone function. *Invest Ophthalmol Vis Sci*. 2001;42:506–513.

5. Toda K, Bush RA, Humphries P, Sieving PA. The electroretinogram of the rhodopsin knockout mouse. *Vis Neurosci*. 1999;16:391–398.

6. Wang R, Jiang C, Ma J, Young MJ. Monitoring morphological changes in the retina of rhodopsin$^{-/-}$ mice with spectral domain optical coherence tomography. *Invest Ophthalmol Vis Sci*. 2012;53:3967–3972.

7. Tanimoto N, Sothilingam V, Kondo M, Biel M, Humphries P, Seeliger MW. Electroretinographic assessment of rod- and cone-mediated bipolar cell pathways using flicker stimuli in mice. *Sci Rep*. 2015;5:10731.

8. Grover S, Fishman GA, Alexander KR, Anderson RJ, Derlacki DJ. Visual acuity impairment in patients with retinitis pigmentosa. *Ophthalmology*. 1996;103:1593–1600.

9. Prusky GT, Alam NM, Beekman S, Douglas RM. Rapid quantification of adult and developing mouse spatial vision using a virtual optomotor system. *Invest Ophthalmol Vis Sci*. 2004;45:4611–4616.

10. McNally N, Kenna P, Humphries MM, et al. Structural and functional rescue of murine rod photoreceptors by human rhodopsin transgene. *Hum Mol Genet*. 1999;8:1309–1312.

11. Liang Y, Fotiadis D, Maeda T, et al. Rhodopsin signaling and organization in heterozygote rhodopsin knockout mice. *J Biol Chem*. 2004;279:48189–48196.

12. Chakraborty D, Ding XQ, Fliesler SJ, Naash MI. Outer segment oligomerization of Rds: evidence from mouse models and subcellular fractionation. *Biochemistry*. 2008;47:1144–1156.

13. Huber G, Beck SC, Grimm C, et al. Spectral domain optical coherence tomography in mouse models of retinal degeneration. *Invest Ophthalmol Vis Sci*. 2009;50:5888–5895.

14. Berger A, Cavallero S, Dominguez E, et al. Spectral-domain optical coherence tomography of the rodent eye: highlighting layers of the outer retina using signal averaging and comparison with histology. *PLoS One*. 2014;9:e96494.

15. Dai X, Zhang H, He Y, Qi Y, Chang B, Pang JJ. The frequency-response electroretinogram distinguishes cone and abnormal rod function in rd12 mice. *PLoS One*. 2015;10: e0117570.

16. Shi C, Yuan X, Chang K, et al. Optimization of optomotor response-based visual function assessment in mice. *Sci Rep*. 2018;8:9708.

17. Cahill H, Nathans J. The optokinetic reflex as a tool for quantitative analyses of nervous system function in mice: application to genetic and drug-induced variation. *PLoS One*. 2008;3:e2055.

18. Tabata H, Shimizu N, Wada Y, Miura K, Kawano K. Initiation of the optokinetic response (OKR) in mice. *J Vis*. 2010;10(1): 13.

19. Thaung C, Arnold K, Jackson IJ, Coffey PJ. Presence of visual head tracking differentiates normal sighted from retinal degenerate mice. *Neurosci Lett*. 2002;325:21–24.

20. Kretschmer F, Sajgo S, Kretschmer V, Badea TC. A system to measure the optokinetic and optomotor response in mice. *J Neurosci Methods*. 2015;256:91–105.

21. Simpson JI. The accessory optic system. *Annu Rev Neurosci*. 1984;7:13–41.

22. Umino Y, Solessio E. Loss of scotopic contrast sensitivity in the optomotor response of diabetic mice. *Invest Ophthalmol Vis Sci*. 2013;54:1536–1543.

23. Barabas P, Huang W, Chen H, et al. Missing optomotor head-turning reflex in the DBA/2J mouse. *Invest Ophthalmol Vis Sci*. 2011;52:6766–6773.

24. Douglas RM, Alam NM, Silver BD, McGill TJ, Tschetter WW, Prusky GT. Independent visual threshold measurements in the two eyes of freely moving rats and mice using a virtual-reality optokinetic system. *Vis Neurosci*. 2005;22:677–684.

25. Akimov NP, Renteria RC. Spatial frequency threshold and contrast sensitivity of an optomotor behavior are impaired in the Ins2Akita mouse model of diabetes. *Behav Brain Res*. 2012;226:601–605.

26. Redfern WS, Storey S, Tse K, et al. Evaluation of a convenient method of assessing rodent visual function in safety pharmacology studies: effects of sodium iodate on visual acuity and retinal morphology in albino and pigmented rats and mice. *J Pharmacol Toxicol Methods*. 2011;63:102–114.

27. Rangarajan KV, Lawhn-Heath C, Feng L, Kim TS, Cang J, Liu X. Detection of visual deficits in aging DBA/2J mice by two behavioral assays. *Curr Eye Res*. 2011;36:481–491.

28. Yang Q, Cho KS, Chen H, et al. Microbead-induced ocular hypertensive mouse model for screening and testing of aqueous production suppressants for glaucoma. *Invest Ophthalmol Vis Sci*. 2012;53:3733–3741.

29. Schneider CA, Rasband WS, Eliceiri KW. NIH Image to ImageJ: 25 years of image analysis. *Nat Methods*. 2012;9:671–675.

30. Yu D, Zheng J, Zhu R, et al. Computer-aided analyses of mouse retinal OCT images - an actual application report. *Ophthalmic Physiol Opt*. 2015;35:442–449.

31. Yang L, Kim JH, Kovacs KD, Arroyo JG, Chen DF. Minocycline inhibition of photoreceptor degeneration. *Arch Ophthalmol*. 2009;127:1475–1480.

32. Altimus CM, Guler AD, Alam NM, et al. Rod photoreceptors drive circadian photoentrainment across a wide range of light intensities. *Nat Neurosci*. 2010;13:1107–1112.

33. Dedek K, Pandarinath C, Alam NM, et al. Ganglion cell adaptability: does the coupling of horizontal cells play a role? *PLoS One*. 2008;3:e1714.

34. Oyster CW, Simpson JI, Takahashi ES, Soodak RE. Retinal ganglion cells projecting to the rabbit accessory optic system. *J Comp Neurol*. 1980;190:49–61.

35. Yonehara K, Shintani T, Suzuki R, et al. Expression of SPIG1 reveals development of a retinal ganglion cell subtype projecting to the medial terminal nucleus in the mouse. *PLoS One*. 2008;3:e1533.

36. Schmucker C, Seeliger M, Humphries P, Biel M, Schaeffel F. Grating acuity at different luminances in wild-type mice and in mice lacking rod or cone function. *Invest Ophthalmol Vis Sci*. 2005;46:398–407.

37. Alexander KR, Derlacki DJ, Fishman GA. Contrast thresholds for letter identification in retinitis pigmentosa. *Invest Ophthalmol Vis Sci*. 1992;33:1846–1852.

38. Alexander KR, Derlacki DJ, Fishman GA. Visual acuity vs letter contrast sensitivity in retinitis pigmentosa. *Vision Res*. 1995; 35:1495–1499.

39. Akeo K, Hiida Y, Saga M, Inoue R, Oguchi Y. Correlation between contrast sensitivity and visual acuity in retinitis pigmentosa patients. *Ophthalmologica*. 2002;216:185–191.

40. Oomachi K, Ogata K, Sugawara T, Hagiwara A, Hata A, Yamamoto S. Evaluation of contrast visual acuity in patients with retinitis pigmentosa. *Clin Ophthalmol*. 2011;5:1459–1463.

41. Oishi M, Nakamura H, Hangai M, Oishi A, Otani A, Yoshimura N. Contrast visual acuity in patients with retinitis pigmentosa assessed by a contrast sensitivity tester. *Indian J Ophthalmol*. 2012;60:545–549.

42. Lindberg CR, Fishman GA, Anderson RJ, Vasquez V. Contrast sensitivity in retinitis pigmentosa. *Br J Ophthalmol*. 1981;65: 855–858.

43. Lem J, Krasnoperova NV, Calvert PD, et al. Morphological, physiological, and biochemical changes in rhodopsin knock-out mice. *Proc Natl Acad Sci U S A*. 1999;96:736–741.

44. Soto F, Kerschensteiner D. Synaptic remodeling of neuronal circuits in early retinal degeneration. *Front Cell Neurosci*. 2015;9:395.

45. Peng YW, Hao Y, Petters RM, Wong F. Ectopic synaptogenesis in the mammalian retina caused by rod photoreceptor-specific mutations. *Nat Neurosci*. 2000;3:1121–1127.

46. Haq W, Arango-Gonzalez B, Zrenner E, Euler T, Schubert T. Synaptic remodeling generates synchronous oscillations in the degenerated outer mouse retina. *Front Neural Circuits*. 2014;8:108.

47. Haverkamp S, Michalakis S, Claes E, et al. Synaptic plasticity in CNGA3(-/-) mice: cone bipolar cells react on the missing cone input and form ectopic synapses with rods. *J Neurosci*. 2006; 26:5248–5255.

48. Strettoi E, Pignatelli V. Modifications of retinal neurons in a mouse model of retinitis pigmentosa. *Proc Natl Acad Sci U S A*. 2000;97:11020–11025.

49. Claes E, Seeliger M, Michalakis S, Biel M, Humphries P, Haverkamp S. Morphological characterization of the retina of the CNGA3(-/-)Rho(-/-) mutant mouse lacking functional cones and rods. *Invest Ophthalmol Vis Sci*. 2004;45:2039–2048.

50. Strettoi E, Pignatelli V, Rossi C, Porciatti V, Falsini B. Remodeling of second-order neurons in the retina of rd/rd mutant mice. *Vision Res*. 2003;43:867–877.

51. Phillips MJ, Otteson DC, Sherry DM. Progression of neuronal and synaptic remodeling in the rd10 mouse model of retinitis pigmentosa. *J Comp Neurol*. 2010;518:2071–2089.

52. Zhang T, Zhang N, Baehr W, Fu Y. Cone opsin determines the time course of cone photoreceptor degeneration in Leber congenital amaurosis. *Proc Natl Acad Sci U S A*. 2011;108: 8879–8884.

53. Menghini M, Lujan BJ, Zayit-Soudry S, et al. Correlation of outer nuclear layer thickness with cone density values in patients with retinitis pigmentosa and healthy subjects. *Invest Ophthalmol Vis Sci*. 2014;56:372–381.

54. Punzo C, Kornacker K, Cepko CL. Stimulation of the insulin/mTOR pathway delays cone death in a mouse model of retinitis pigmentosa. *Nat Neurosci*. 2009;12:44–52.

55. Gresh J, Goletz PW, Crouch RK, Rohrer B. Structure-function analysis of rods and cones in juvenile, adult, and aged C57bl/6 and Balb/c mice. *Vis Neurosci*. 2003;20:211–220.

56. Huberman AD, Niell CM. What can mice tell us about how vision works? *Trends Neurosci*. 2011;34:464–473.

57. Wolkstein M, Atkin A, Bodis-Wollner I. Contrast sensitivity in retinal disease. *Ophthalmology*. 1980;87:1140–1149.

58. Jindra LF, Zemon V. Contrast sensitivity testing: a more complete assessment of vision. *J Cataract Refract Surg*. 1989; 15:141–148.

59. Ratnam K, Carroll J, Porco TC, Duncan JL, Roorda A. Relationship between foveal cone structure and clinical measures of visual function in patients with inherited retinal degenerations. *Invest Ophthalmol Vis Sci*. 2013;54:5836–5847.